Numerical simulations of internal nozzle flow in a pressure swirl atomizer for aircraft engines

C. Galbiati[1], S. Tonini[2], P. Conti[3], G.E. Cossali[4]
University of Bergamo, 24044 Dalmine, Italy

The internal flow and the liquid structure *at nozzle exit* are investigated in a typical pressure swirl atomizer for aero-engine applications under isothermal non reacting environment, using a two-phase flow modeling according to the VOF numerical methodology. A parametrical analysis is performed to investigate the effect of operating conditions on the injector performances and the characteristics of the liquid jet exiting the nozzle. The liquid film thickness at nozzle exit and the injector discharge coefficient predicted by the simulations are compared against commonly used correlations available in the literature. The influence of the turbulence model on the injector performances is also analyzed using three different models: the RNG k-ε model, the Reynolds Stress Model (RSM) and the Large Eddy Simulation (LES) model.

Nomenclature

Roman symbols

A_o	discharge orifice area, m^2
A_p	*total* inlet port area, m^2
C_D	discharge coefficient
d_{Hi}	*inlet channel hydraulic diameter*
d_m	*twice the distance between the inlet port centre and the nozzle axis, m*
d_o	discharge orifice diameter, m
d_s	swirl chamber diameter, m
FN	flow number, m^2

[1] PhD student, Department of Engineering and Applied Sciences, Viale Marconi Dalmine (BG), Italy.
[2] Research assistant, Department of Engineering and Applied Sciences, Viale Marconi Dalmine (BG), Italy.
[3] Technician, Department of Engineering and Applied Sciences, Viale Marconi Dalmine (BG), Italy.
[4] Professor, Department of Engineering and Applied Sciences, Viale Marconi Dalmine (BG), Italy.

G_z	*flux of momentum, kg m/s²*
K	atomizer constant
K_v	*velocity coefficient*
l	*length, m*
$\dot{m}_l$	liquid flow rate, kg/s
M_θ	*axial flux of angular momentum, kg m²/s²*
P	*pressure, Pa*
Re_o	Reynolds number *at nozzle exit*
Re_W	*Reynolds number according to Walzel definition [1]*
R_o	discharge orifice radius, m
SN	*Swirl number*
t	film thickness, m
U	*velocity, m/s*
$X,\ \tilde{X}$	area ratios
z	injector axis coordinate, m

Greek symbols

β	*swirl chamber angle, degree*
ΔP	*pressure drop across the PSA, Pa*
ΔP_{hole}	*pressure drop across the discharge hole, Pa*
μ	dynamic viscosity, kg/ms
ρ	density, kg/m^3
σ	surface tension, kg/s^2

Subscripts

g	*gas*
l	*liquid*
o	*discharge hole exit section*
s	*swirl chamber*

Abbreviation

ARMS	*Algebraic Reynolds Stress Model*
CFD	*Computational Fluid Dynamics*
CICSAM	*Compressive Interface Capturing Scheme for Arbitrary Meshes*
LDA	*Laser Doppler Anemometry*
LES	*Large Eddy Simulation*
PSA	*Pressure Swirl Atomiser*
RMS	*Root Mean Square*
RNG	*Re-Normalisation Group*
RSM	*Reynolds Stress Model*

I. Introduction

Pressure swirl atomizers (PSAs) are widely used in combustion systems such as gas turbine engines, internal combustion engines and boilers, to obtain good quality of mixing between oxidant and fuel with low injection energy as well as simple and inexpensive manufacturing. In order to produce a controlled spray that reduces the NOx concentration during the combustion process, it is necessary to predict with high accuracy the atomizer performances. A typical PSA is composed by various tangential ports feeding the fuel to the internal chamber and creating a swirling flow in the atomizer; the liquid rotation inside the exit orifice displaces the liquid near the wall [2], creating a depression within the internal region that causes the entrainment of the external gas and the formation of a gas core inside the hole.

In the open literature many correlations are available, see [2] for a general review, which allow to estimate the value of the characteristic parameters describing the behavior of these atomizers, namely: the liquid lamella thickness at the exit section of the atomizer, the discharge coefficient and the spray cone angle. All the correlations reported by [2] were developed by fitting ad-hoc experimental results and include the operating conditions, in terms of pressure drop and mass flow rate, the liquid properties and the geometrical characteristics of the atomizer. It should be noticed that not all the correlations are suitable for all the adopted configurations since they were developed only for specific atomizer topologies.

To better understand the link between the internal flow and the atomizer outcomes, some authors have performed flow visualizations and velocity measurements on large scale PSA. LDA measurements on a classical geometry

were conducted by [3, 4], testing the effect of the fuel viscosity. Under low Reynolds number conditions, the experiments show that the axial liquid velocity profile inside the nozzle has one small peak close to the wall, which disappears at high Reynolds numbers. The tangential velocity profile measured in front of the inlet ports and at the centre of the swirl chamber reveals the influence of the boundary layer developed into the inlet channels, which reduces the effective cross-sectional area at the nozzle exit. A more recent study, made by [5], includes LDA measurements and visualizations of the internal flow field. Their results show a characteristic shape of the liquid stream axial velocity profile at the inlet port (corresponding to the exit section of the inlet channels), where two velocity peaks were found: one close to the wall and the other one in correspondence of the interface between the liquid and the air-core confirming the observations of [6] in a similar flow. Donjat et al. [5-7] found two dominant instabilities moving along the interface of the air-core: the first one, at lower frequency, is associated to the precession mode, whereas the second one, at higher frequency, is associated to the helical mode. Both these instabilities grow when the fluid reaches the convergent section of the atomizer, and this phenomenon is enhanced as the flow rate increases. The authors concluded that the development of these instabilities strongly depends on the inlet port geometry and on the size of the outlet section of the nozzle.

Experiments on a large scale PSA were also carried out to find a way to extrapolate the main parameters by varying the geometrical dimensions of the atomizer. Sumer et al. [8] found that for the classical PSA geometry, composed by two or four inlet ports normal to the axis of the atomizer and a pressure swirl chamber composed by one cylindrical section followed by a conical section, the values of the lamella thickness measured in their experiments are in rather good agreement with the previous correlation proposed by Suyari and Lefebvre [9], while other authors like Benjamin et al. [10, 11] found that the same correlation underestimates the value of the film thickness emerging from the atomizer. *The main differences between the two atomizers are related to the length of the pressure swirl chamber, the number of the inclined channels and the scale of the atomizer: Benjamin et al. [10, 11] used a large injector, with a discharge hole of 18mm, while Sumer et al. [8] used an injector with discharge hole equal to 2mm. Benjamin et al. [10, 11] emphasized that the scale of the atomizer alone may dramatically influence the formation of the air-core within the nozzle discharge hole of an injector compared to another one, even if the non-dimensional numbers generally used to characterize them are comparable.*

The recent advances in CFD methodologies and computational resources have provided another way to characterize the internal flow field in swirling atomizers, and both in-house [10-13] and commercial [4, 5, 8, 14-17]

CFD codes were used to perform the task. The predictions are in rather good agreement with the available experimental results, although they reveal some mismatch with the semi-empirical correlations from the literature, which are nowadays routinely used by the industries to predict the atomizer performances. Hence, the major limit of the semi-empirical correlations describing typical PSAs is that they yield acceptable predictions only for the geometries and the scales adopted to develop them. Unfortunately, the number of possible configurations is significant and consequently it is not possible to define a universal law that reasonably predicts the behavior of any atomizer. This underlines the importance of detailed experimental and numerical investigations of the internal flow field to correlate the atomizer outcomes with its geometrical configuration.

The presence of a swirling flow in a convex surface chamber with high curvature adds a complexity to the problem since the choice of a turbulence model may influence the CFD predictions. Yeh [18] and Madsen et al. [17] performed a comparison among different turbulence models on two different pressure swirl atomizers, by using the VOF methodology. In particular, Yeh [18] tested two low Reynolds number k-ε models (Launder-Sharma's LNR model and Nagano-Hishida's LNR model) and Gatski-Speziale algebraic Reynolds stress model (ARSM). The final comparison with different experiments found in literature evidenced that the turbulence intensity seems to have a significant role on the global characteristics of the flow field and the Gatski-Speziale ARMS turbulence model seems to better predict this parameter. Hence, Yeh [18] concluded that this should be preferred to describe the main characteristics of the PSA, confirming that the standard k-ε model overestimates the turbulence intensity, leading to a poor estimation of the swirled flow characteristics. *Madsen et al. [17] proposed a campaign of numerical simulations with different turbulence models implemented in commercial CFD codes on a large scale PSA, using computational grids up to about 600,000 cells. They used different numerical methods: a) laminar flow assumption using VOF and Euler/Euler methodologies; b) standard RNG and realizable two-equation k-ε turbulence models; c) VOF LES (Large Eddies Simulation). They found that the simulations using the standard RNG and the realizable two-equations k-ε model were not capable to predict the existence of the air core inside the exit hole observed in the experiments made by Hansen [16] on the same injector. The simulations performed assuming laminar flow and LES methodology were capable to qualitatively reproduce the main topological characteristics of the flow inside the nozzle, however they pointed out the necessity of grid refinement.*

The present work reports the results from numerical investigation on a small scale atomizer for aeronautical applications, with a geometry similar to the one studied in [16, 17], but with four feed slots positioned at the top of a

conical swirl chamber. *To overcome the previously mentioned grid resolution problem, computational grids up to 12 million cells were used.*

All the effort made to study this kind of atomizer over the years is to better understand, and consequently control, the production of the spray inside the combustion chamber of aircraft engines, in order to reduce the production of NOx during the combustion. Since the development of the jet and its successive atomization depend on the characteristics of the annular liquid film formed at the exit section of the nozzle, it is crucial to investigate the internal flow field to better understand the characteristics of the final spray. The work reported in this paper is aimed to give an overview of the flow behavior inside this kind of injector under a wide range of operating conditions typical of aeronautical applications using different CFD models.

In the next sections of the paper the implemented numerical methodology is briefly presented, followed by the discussion of the main results and the summary of the most important conclusions.

II. Mathematical modeling and numerical set-up

The flow development inside the injector and at the nozzle exit proximity is predicted implementing the two-phase flow VOF (Volume of Fluid) methodology [19]. The CFD model numerically solves the fully 3D Navier-Stokes equations describing the fluid motion, with the time averaged forms of the continuity, momentum and conservation equations for the scalar variables using collocated Cartesian velocity components on structured and unstructured numerical grids. *The flow is assumed to be incompressible under iso-thermal non-reacting conditions.* The discretization method is based on the finite volume approach and the pressure correction method is according to the SIMPLE algorithm; high resolution hybrid and CICSAM (Compressive Interface Capturing Scheme for Arbitrary Meshes) schemes are adopted for the spatial discretization, while the time discretization is based on a fully implicit Crank-Nicolson scheme. The first order standard RNG k-ε model, the second order Reynolds Stress Model (RSM) and the Large Eddy Simulation model (LES) are used to include the effect of turbulence [20]. *Within each time step, the residuals in the calculation of the various flow variables have been monitored and residual values less than 1.E-3 were selected as convergence criteria. Since the inlet mass flow and the back pressure are kept constant, the simulations were stopped when a quasi-steady solution was reached. Such condition is assumed to be achieved when the fluctuation amplitudes of the key macroscopic flow parameters, i.e. the liquid lamella thickness, the averaged liquid swirl velocity at nozzle exit and the pressure drop across the discharge hole, stabilize. The above*

mentioned parameters were selected since they are the main input of available primary atomization models, which link the inner flow to the spray formation.

A. Computational domain and operating conditions

The computational domain is composed by three sections (see Fig. 1): the first one corresponds to the connection between the feeding line of the system and the second section that represents the core of the pressure swirl atomizer. *The last part (section # 3) represents the external chamber, made by a cylindrical body with a diameter equals to 16 times the diameter of the nozzle discharge hole (d_o) and with height equal to $8d_o$. The dimension of the cylindrical domain selected to simulate the flow outside the nozzle has been chosen to minimize its influence on the predictions. Preliminary tests were performed to select the final extent. It should be noticed that the present investigation is fully focused on the internal nozzle flow and the flow at the nozzle exit proximity, without any attempts to predict the spray formation and evolution.*

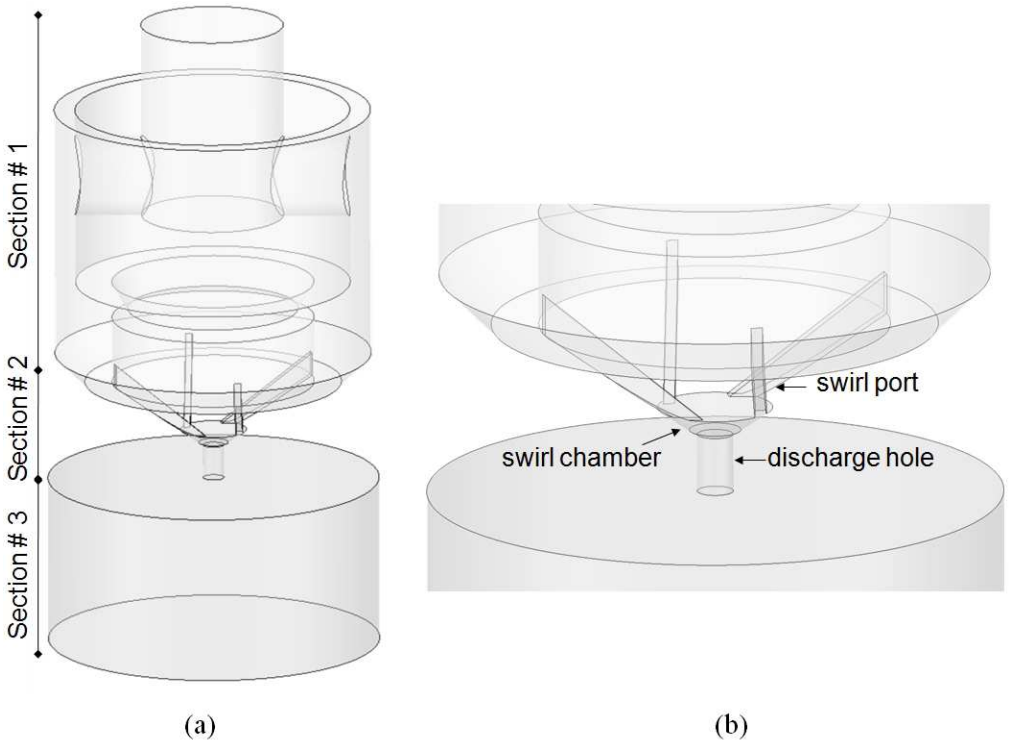

Fig. 1 (a) Whole computational domain and (b) zoom on pressure swirl atomizer section.

The pressure swirl atomizer (section # 2) is composed by three elements: the four inclined swirling channels, the swirling chamber and the fuel discharge hole, which dimensions are reported in Fig. 2, together with the values of the total port area (A_p) at the channel exit section, the hydraulic diameter d_{Hi} of each inlet channel and d_m, which is twice the distance between the inlet port centre and the nozzle axis. The four inclided swirling channels are tangent to the pressure swirl chamber external wall, with an injection angle of 54° respect to the atomizer axis.

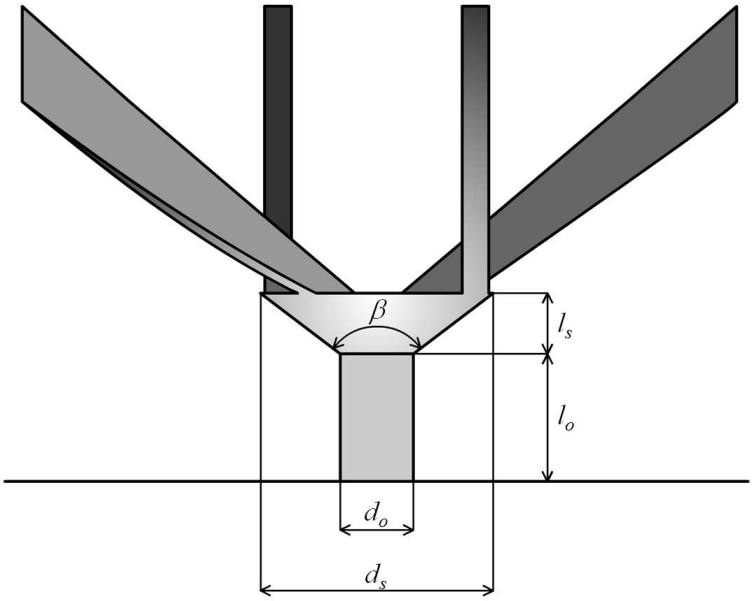

Fig. 2 Pressure swirl atomizer geometrical characteristics.

Parameter	Value
β	116°
d_o [m]	0.625E-3
d_s [m]	2.000E-3
l_o [m]	1.072E-3
l_s [m]	0.428E-3
d_m [m]	1.800E-3
A_p [m^2]	0.288E-6
d_{Hi} [m^2]	0.230E-3

Hybrid 3D grids were created, made by tetrahedral, hexahedral and prismatic cells; the tetrahedral elements were used to mesh the inclined channels of the PSA and the subsequent insertion into the swirling chamber; the remaining part of the domain was meshed with hexahedral or prismatic cells (see Fig. 3). *A grid dependence analysis was carried out adopting the grid structure described above, but with a different number of cells, starting with 1 million up to 12 millions [21]. A comparison in terms of pressure drop across the discharge hole and the values of liquid lamella thickness and averaged swirl velocity at the exit section of the atomizer shows that an acceptable grid independency is achieved with grids made by more than 8 million cells. To achieve a better spatial accuracy, all the simulations with the LES model were performed using a finer grid with 12 million cells, adopting the Smagorinsky-*

Lilly subgrid-scale model [22]. The simulations with the RNG k-ε model and the Reynolds Stress Model were performed on the relatively coarser grid with 8 million cells, to reduce the computational time.

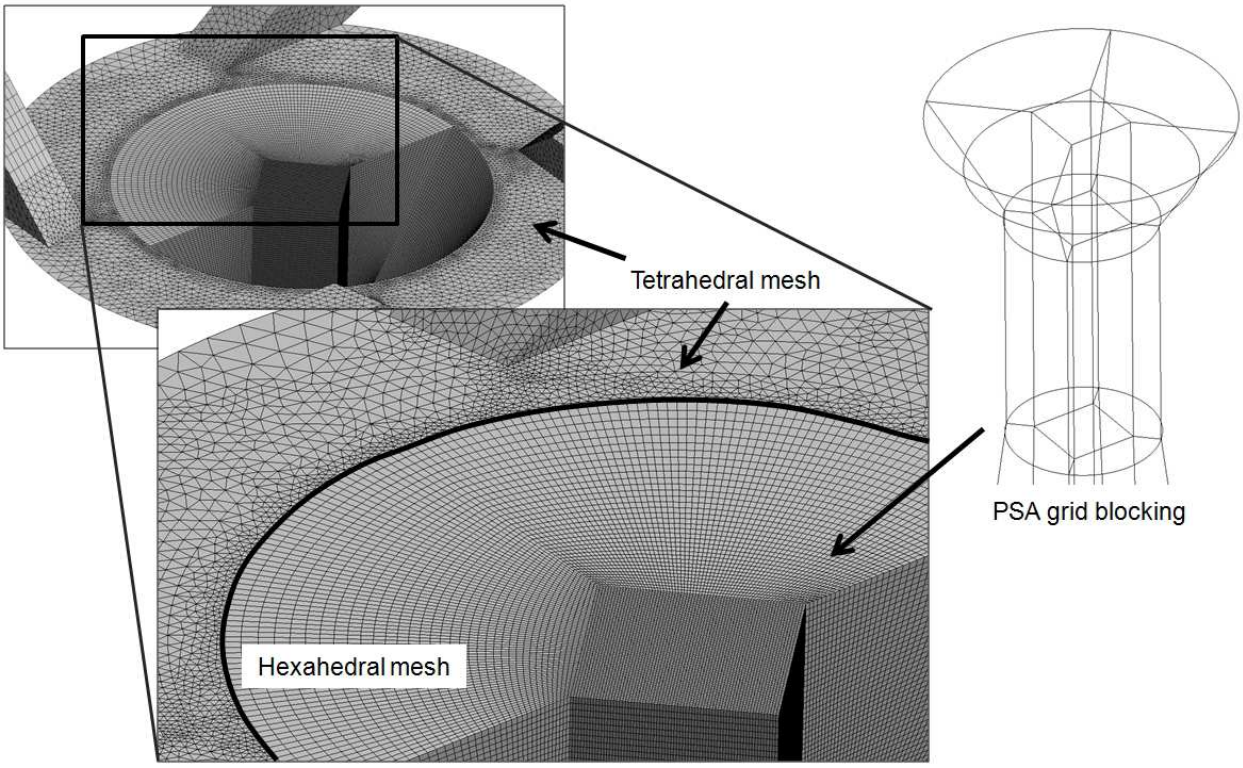

Fig. 3 Grid blocking and details of the computational mesh.

As boundary conditions, the fuel mass flow rate was set constant at the inlet section, *while uniform and constant pressure was imposed at outflow boundaries. Eight operating conditions were selected, corresponding to different test cases for a typical aircraft engine. Table 1 reports the operating conditions for the selected cases, corresponding to the injection fuel flow rate and the gas back pressure and density, together with the corresponding values of the Reynolds number evaluated at the nozzle exit section, defined as:*

$$\mathrm{Re}_o = \frac{\rho_l U_o d_o}{\mu_l} \qquad (1.a)$$

$$U_o = \frac{4\dot{m}_l}{\pi d_o^2 \rho_l} \qquad (1.b)$$

The fuel is modeled using the physical properties of Kerosene jet-A1, as listed in Table 2. *The fuel Jet A-1 is a mixture of a large number of different hydrocarbons, with a carbon number distribution between about 8 and 16. Its critical pressure is 2.344MPa and critical temperature is 684.26K [23]. Since no experimental data on the fuel temperature variation through the nozzle are available, all the simulations were performed imposing adiabatic flow, i.e. no heating of fuel from the initial temperature was considered, thus neglecting possible heat transfer through the PSA walls or heat exchange with the surrounding gas. The fuel temperature is considered constantly equal to the inlet temperature, 300K. For n-dodecane, which is one of the main fuel components, the density at 0.1MPa and 4MPa differs by less than 0.3%, at 300K. Moreover, the sound speed in n-dodecane at 300K is equal to 1273m/s at 0.1MPa and 1297m/s at 4MPa, then, being the maximum fuel velocity lower than 30m/s, the corresponding Mach number further justifies the incompressibility assumption. On the same basis, the supercritical behavior of the fuel in some of the reported test-cases has been ignored. Surface tension is taken into account in the momentum equation as a surface force according to the CSF (Continuum Surface Forces) model [24]. In the reported simulations the value of surface tension at 300K, equal to 0.022kg/m^2, is used. It must be noticed that the only region where surface tension may play a role in the in-nozzle flow is in correspondence of the air-core fuel interface. However, the estimated Weber number in this region is larger than 10000, evidencing that capillarity effect plays a very marginal role in defining the interface topology and the flow field. Thus the effect of possible variation of surface tension with pressure and temperature is expected to be marginal.*

The two-phase flow modeling adopted for the purposes of the present investigation required transient simulations to be performed, whereas the predicted flow was assumed to be under quasi steady-state conditions. As initial condition, the simulation imposes the liquid occupying the whole injector, and the subsequent formation of the air core is calculated.

The lamella thickness and velocity at the discharge hole exit and the liquid pressure drop across the discharge hole were extracted from the simulations at time steps of 0.1 μs and they were time averaged to account for the temporal fluctuations. A similar procedure was used to estimate the uncertainties of the above mentioned parameters and of the pressure drop across the PSA. The uncertainties due to the temporal fluctuations were found to be less than 6% for the lamella thickness, to be compared with the error due to numerical diffusion that is between 11% and 18% (see Table 3), less than 6% for the fuel velocity and less than 7% and 1% for the pressure drop across the discharge hole and across the PSA, respectively.

Table 1. Test case operating conditions

Case		$\dot{m}_l$ (g/s)	P_g (MPa)	ρ_g (kg/m^3)	Re_o
# 1	Take off (50%)	2.8	3.20	13.3	4388
# 2	Take off (100%)	5.6	3.20	13.3	8776
# 3	Approach (30%)	3.0	1.28	6.8	4701
# 4	Cruise	6.2	1.14	5.5	9716
# 5	Idle (7%)	3.4	0.51	3.4	5328
# 6	Descent Idle	2.8	0.31	1.9	4388
# 7	Low Idle	3.3	0.31	2.4	5171
# 8	Type test	3.4	3.13	12.4	5328

Table 2. Liquid properties of Kerosene jet A-1

Liquid properties	
ρ (kg/m^3)	801
μ (kg/ms)	0.0013
σ (kg/s^2)	0.0225

III. Results and discussion

A sample of the two-phase flow development within the injector and at nozzle exit proximity as predicted with LES turbulence model is reported in Fig. 4. The image corresponds to the test case # 1 of Table 1, showing the liquid swirling flow induced by the four inclined passages and the formation of the lamella at nozzle exit with the liquid/gas interface location.

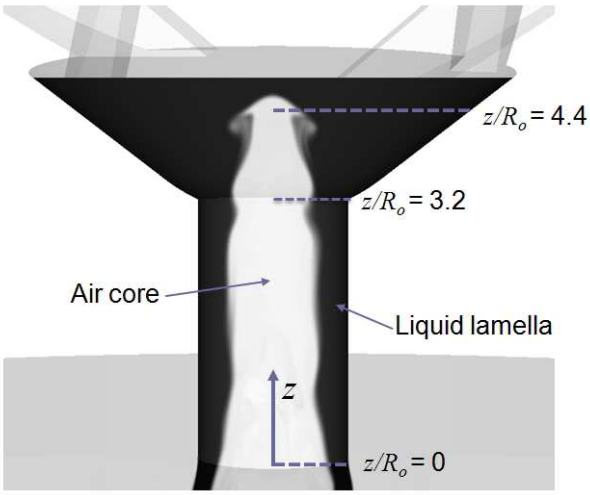

Fig. 4 **Sample of two-phase flow development below the swirling ports; test case # 1 of Table 1.**

A parameter that characterizes a pressure swirl atomizer is the Swirl Number, which is calculated according to the following expression [25]:

$$SN = \frac{M_\vartheta}{R_o G_z} \tag{2}$$

where M_θ and G_z are the axial flux of angular momentum and the flux of momentum, respectively, and they are calculated at the discharge hole exit section, according to the following expressions:

$$G_z = \int_A \rho U_{\text{axial}}^2 dA \tag{3}$$

$$M_\theta = \int_A \rho U_{\text{axial}} U_{swirl} r dA \tag{4}$$

where r is the distance from the injector axis.

The Swirl Number for the selected injector is almost independent of the operating conditions, with a value varying in a range from 0.67 up to 0.81 for the eight test cases reported in Table 2.

In the absence of experimental data that would help in the characterization of the flow in such complex geometry, numerical simulation is the only tool that could provide information of the physical processes occurring and their effect on the fragmentation of the liquid film exiting the nozzle into ligaments and drops. Different computational tools are available in the open scientific literature, however their reliability should be considered together with the requested computational resources, in terms of computational time and hardware resources, related to their use.

The atomization performances of a PSA can be monitored by few macroscopic parameters, which are commonly defined as inputs for the primary atomization models used to predict the drop characteristics formed by the fragmentation of the liquid ligaments exiting the nozzle in contact with the surrounding air. Among them, the most relevant are the thickness of the liquid lamella at the nozzle exit and its velocity *and the pressure drop across the discharge hole*.

Due to the centrifugal force acting on the liquid exiting this type of nozzle, an air core is usually present in the discharge hole, then the evaluation of the liquid lamella thickness at the nozzle exit requires the correct prediction of the liquid/gas interface in this region.

As a consequence of the numerical diffusion in the calculation of the VOF variable, due to the spatial discretization selected for the purposes of the present investigation, the evaluation of the exact location of the gas-liquid interface is affected by numerical error, which should be taken into account in the evaluation of the lamella thickness. Consequently, a mean value for the lamella thickness is calculated, at each time step, defining a mean position of the liquid/gas interface by averaging the values corresponding to five thresholds of the VOF parameter, equal to 0.1, 0.25, 0.5, 0.75 and 0.9. The evaluation of the RMS (root mean square) quantifies the inaccuracy of the lamella thickness estimation.

Table 3 reports the values of the mean liquid lamella thickness and its RMS for the eight selected test cases together with the corresponding values of the liquid swirl velocity at nozzle exit and the liquid pressure drop across the discharge hole. The results evidence the predictable increase of the liquid swirl velocity and the pressure drop across the hole with the mass flow rate, while the lamella thickness, which is expected to depend on many parameters, does not show any monotonic dependence on mass flow rate.

Several correlations are available in the literature to describe typical PSA performances, but no universal law exists to account for all the PSA geometries and operating conditions. Table 4 reports the five correlations, widely used to predict the film thickness t at nozzle exit [2, 9, 10, 26, 27].

Figure 5 shows the comparison of the mean values of liquid lamella thickness extracted from the simulations (the error bars refer to the above mentioned RMS) and the values predicted by the reported correlations (see Table 4).

Table 3. Values of lamella thickness and liquid swirl velocity at nozzle exit and liquid pressure drop across the nozzle discharge hole for the eight test cases of Table 1.

Case		t (μm)	RMS$_t$ (μm)	U_{swirl} (m/s)	ΔP_{hole} (MPa)
1	Take off (50%)	102.0	11.1	13.8	0.143
2	Take off (100%)	88.8	15.7	35.6	0.603
3	Approach (30%)	95.6	9.9	16.2	0.184
4	Cruise	87.8	13.7	41.3	0.772
5	Idle (7%)	95.7	10.8	18.8	0.229
6	Descent Idle	88.7	11.4	16.2	0.164
7	Low Idle	95.4	11.7	18.9	0.222
8	Type test	108.8	11.6	16.0	0.179

Table 4. Correlations for fuel thickness at nozzle exit in pressure swirl atomizers

	Reference	Correlation	Experimental conditions
From potential theory	Giffen and Muraszew [27]	$\left(\frac{A_p}{d_s d_0}\right)^2 = \frac{\pi}{32}\frac{(1-X)^3}{X^2}$	
	Lefebvre [1]	$\frac{(1-X)^3}{1+X} = 0.09\frac{A_p}{d_s d_0}\left(\frac{d_s}{d_0}\right)^{0.5}$	
Semi-empirical correlations	Rizk and Lefebvre [26]	$t^2 = \frac{1560\dot{m}_l\mu_l}{\rho_l d_o \Delta P}\frac{1+X}{(1-X)^2}$	$0.69MPa < \Delta P < 2.70MPa$ $P_g = 101.3kPa$ $8.0mm < d_s < 10.0mm$ $1.2mm < d_o < 2.4mm$
	Suyari and Lefebvre [8]	$t = 2.7\left[\frac{d_0 FN\mu_l}{(\Delta P\rho_l)^{0.5}}\right]^{0.25}$	
	Benjamin et al. [9]	$t = 0.253K^{0.33}\Delta P^{-0.077}FN^{-0.4}$	$0.069MPa < \Delta P < 0.345MP$ $d_s = 76mm, d_o = 18mm$
	Notes $X = \frac{(d_0-2t)^2}{d_0^2}$; $FN = \frac{\dot{m}_l}{\sqrt{\rho_l\Delta P}}$; $K = \frac{A_p}{d_s d_o}$		

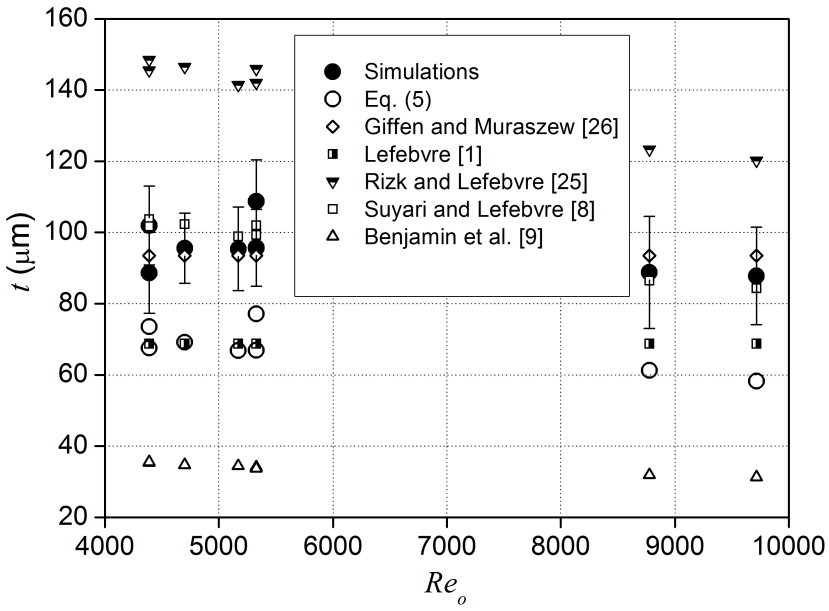

Fig. 5 Effect of *Reynolds number* on the liquid lamella thickness at the discharge hole exit, predicted by LES numerical simulations and by available correlations.

The values of the lamella thickness predicted by the simulations are in rather good agreement with the Giffen and Muraszew [27] and Suyari and Lefebvre [9] correlations. Jedelsky and Jicha [28] suggested the following relationship among the liquid lamella thickness, the liquid velocity and the PSA pressure drop:

$$t = \frac{\dot{m}_l}{\pi d_o K_v^2 \sqrt{2\rho_l \Delta P}} \qquad (5)$$

where K_v is the liquid velocity coefficient, defined as the ratio between the actual liquid velocity at nozzle exit and the Bernoulli velocity. The estimated values of t, obtained with equation (5) and reported in Figure 5, are about 30% lower than those predicted by the simulations.

As previously remarked, the Benjamin's semi-empirical correlation was obtained from experiments on larger size atomizer. The film thickness calculated from this correlation, when applied to a smaller size atomizer, is markedly lower than the values predicted by the other correlations and by the numerical simulations performed in this work. This suggests that there may be some other non-dimensional parameters that are not taken into account. These 'hidden' non-dimensional numbers possibly describe some flow phenomena (~~gravity effect,~~ cavitation, fluid flow detachment to cite a few) that may be responsible for the reported differences in the film thickness at nozzle exit.

The performances of a PSA are usually characterized by the discharge coefficient, which is a function of nozzle geometry and operating conditions. *The commonly accepted definition of the discharge coefficient is the following:*

$$C_D = \frac{\dot{m}_l}{A_o\sqrt{2\rho_l \Delta P}} \tag{6}$$

The values of the pressure drop across the PSA were predicted by the numerical simulations for the eight test cases of Table 1 and the corresponding values of the discharge coefficient are calculated using equation (6) and reported in Fig. 6. The figure also shows the value of C_D calculated from widely used correlations available in the literature, derived for similar injectors [26, 27, 29-31], and reported in Table 5.

As expected for these operating conditions (high Reynolds number >4000), the discharge coefficient predicted by the simulations is almost independent of the operating conditions [32], since viscous effects are expected to be of minor importance and the results from the simulations compare well with all the predictions from the available correlations.

Table 5. Correlations for injector discharge coefficient in pressure swirl atomizers

	Reference	Correlation	
From potential theory	Taylor [30]	$C_D^2 = 0.225\frac{A_p}{d_s d_o}$	
	Giffen and Muraszew [27]	$C_D = 1.17\left[\frac{\left(1-\tilde{X}\right)^3}{1+\tilde{X}}\right]^{0.5}$	$2\left(\pi K/4\right)^2 \tilde{X}^2 = \left(1-\tilde{X}\right)^3$
Semi-empirical correlations	Carlisle [29]	$C_D^2 = 0.0616\frac{d_s}{d_o}\frac{A_p}{d_s d_o}$	
	Rizk and Lefebvre [26]	$C_D = 0.35\left(\frac{A_p}{d_s d_o}\right)^{0.5}\left(\frac{d_s}{d_o}\right)^{0.25}$	
	Babu et al. [31]	$C_D = \frac{K_{C_D}}{\left[\frac{1}{\left(1-X\right)^2} + \frac{\left(\frac{\pi}{4B}\right)^2}{X^n}\right]^{0.5}}$	
	Notes		

$$K_{cd} = 7.3423 \frac{A_o^{0.13735} \left(\frac{\pi d_s^{\,2}}{4} \right)^{0.07782}}{A_p^{0.041066}}; \; B = \frac{A_p}{d_m d_o} \left(\frac{d_m}{d_o} \right)^{1-n};$$

$$n = \begin{cases} 17.57 A_o^{\,0.1396} A_p^{0.2336} \left(\frac{\pi d_s^{\,2}}{4} \right)^{-0.1775} & for \; \Delta P > 2.76 MPa \\ 28 A_o^{\,0.14176} A_p^{0.27033} \left(\frac{\pi d_s^{\,2}}{4} \right)^{-0.17634} & for \; 0.69 MPa < \Delta P < 2.76 MPa \end{cases}$$

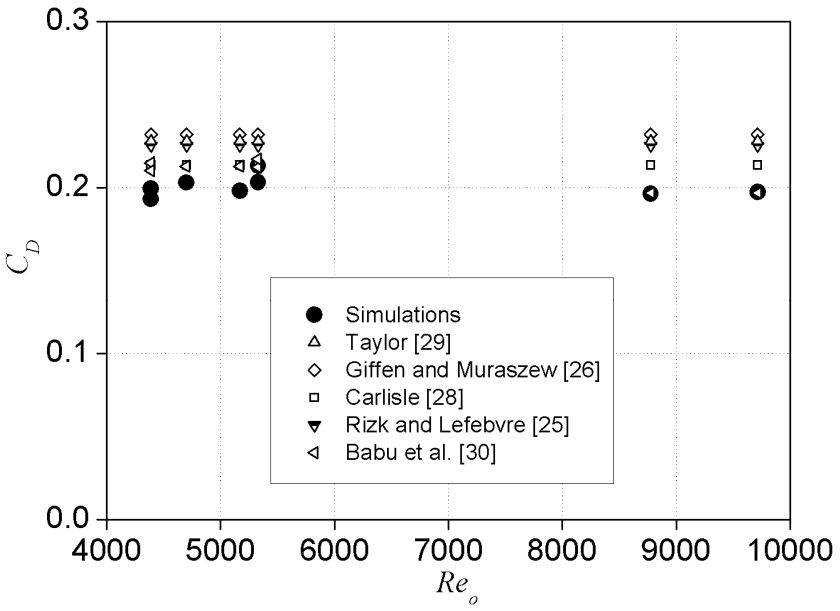

Fig. 6 Effect of *Reynolds number* on the injector discharge coefficient, predicted by LES numerical simulations and by available correlations.

A. Turbulence model investigation

For all the operating conditions reported in Table 1, the value of the Reynolds number calculated using the Walzel definition [1], $\mathrm{Re}_W = \frac{\sqrt{2\rho_l \Delta P} d_o}{\mu_l}$*, ranges from about 17000 up to about 42000, confirming that the flow is fully turbulent, being* Re_W *higher than 5000. Therefore the use of a turbulence model is needed, however the existing experiences [16-18] were not conclusive to define the most appropriate turbulence model for this kind of applications.*

All the results reported in the previous section were obtained using the LES model; this sub-section presents a discussion on the effect of different turbulence models, selected among those that were suggested by previous investigation to be capable to catch the flow behavior for this kind of geometry.

It should be pointed out that experimental data for this injector under the selected operating conditions are not available, making impossible the direct validation of the numerical results. For this reason a comparative analysis is recommended and it will be described in this paragraph.

As testing operating condition, test case # 1 of Table 1 was selected and the results from the Large Eddy Simulation were compared with those obtained using the RNG k-ε turbulence model and the Reynolds stress model (RSM). Since the main parameters describing the PSA characteristics are the lamella thickness and the discharge coefficient, the effect of different turbulence modeling on the predictions of those parameters is presented. Again, in the absence of experimental results for this kind of injector, a comparison with the available correlations will be shown.

Table 6 reports the lamella thickness as predicted by the numerical simulations using the three selected turbulence models and as calculated from the five correlations described in Table 4.

Table 6. Film thickness predicted by numerical simulations using the three turbulence models and by available correlations.

t (μm)	Simulations		Giffen and Muraszew [27]	Lefebvre [1]	Rizk and Lefebvre [26]	Suyari and Lefebvre [8]	Benjamin et al. [9]
	mean	RMS_t					
LES	102.0	11.1					
RNG k-ε	112.7	6.9	93.5	68.7	148.6	103.7	35.3
RSM	135.6	5.5					

The effect of turbulence modeling on the numerical simulation results is relatively small, with a maximum discrepancy from an average value less than 16%, which could be partially ascribed to the inaccuracy in evaluating the exact position of the gas/liquid interface due to numerical diffusion (see the second column of Table 6). The lamella thickness values predicted by the three turbulence models range in an interval that is largely comprised within the range of variation of the results obtained from the available correlations.

Table 7 shows the values of C_D from the simulations using the three turbulence models and the calculations from the five correlations reported in Table 5.

To notice that the correlation of Babu et al. [31] depends on the lamella thickness, consequently three values of C_D, corresponding to the lamella thicknesses predicted by the three turbulence models, were calculated.

The results evidence that the discharge coefficient predicted by the simulations is substantially independent on the choice of the turbulence model and the results are in rather good agreement with the calculations from the available correlations.

Table 7. Discharge coefficient predicted by the simulations using the three turbulence models and by available correlations

C_D	Simulations	Taylor [30]	Giffen and Muraszew [27]	Carlisle [29]	Rizk and Lefebvre [26]	Babu et al. [31]
LES	0.200					0.220
RNG k-ε	0.185	0.228	0.232	0.213	0.225	0.222
RSM	0.197					0.221

To deepen the comparative analysis among the effect of the three turbulence models on the internal nozzle flow field predictions, the axial and swirl fuel velocity profiles have been extracted, for the test case # 1 of Table 1, at three different locations in the swirling chamber and in the discharge hole, corresponding to z/R_o equal to 4.4, 3.2 and 0 (see Fig. 4), and the results are plotted in Fig. 7. All the velocities have been normalized using the axial velocity *defined in equation (1.b).*

The axial velocity profile at z/R_o = 4.4 presents two velocity peaks revealing a recirculation field. The first flow stream is located close to the air-core and it has a higher value than the second one, located near the wall. ~~From the observation of the flow field and the streamlines plotted in Fig. 8, it can be inferred that~~ The peak close to the wall is associated to the jet flow coming from the inlet swirling channels, while the peak located close to the air-core is connected to the presence of a top wall flow, which feeds the air-core stream, meaning that a part of the liquid entering in the swirl chamber is forced radially inward due to the presence of the swirl chamber top wall.

This can be better understood observing the vector map on a cross sectional plane shown in Fig. 8: at the swirl chamber top the stream parallel to the wall moves towards the chamber axis, at the interface with the air core the flow is forced to move down, increasing consequentially the axial velocity component. Also the characteristic

mushroom shape of the air core close to the top wall is caused by the interaction with the flow moving downward with the recirculation of the jet from the inlet channels, which indicates a radial inward fluid motion.

The two above described axial velocity peaks remain visible up to the entrance into the cylindrical discharge hole (section at z/R_o = 3.2), where the flow tends to acquire the classical structure of a confined vortex, as described by Escudier [6]. The same results for the axial velocity profile have been found by Donjat and Estivalezes [5], in their experiments made with LDA and PIV techniques on a large scale pressure swirl atomizer with a classical geometry, and also by Madsen et al. [17] with experiments and simulations made on a large scale pressure swirl atomizer with a geometry similar to that investigated in this work.

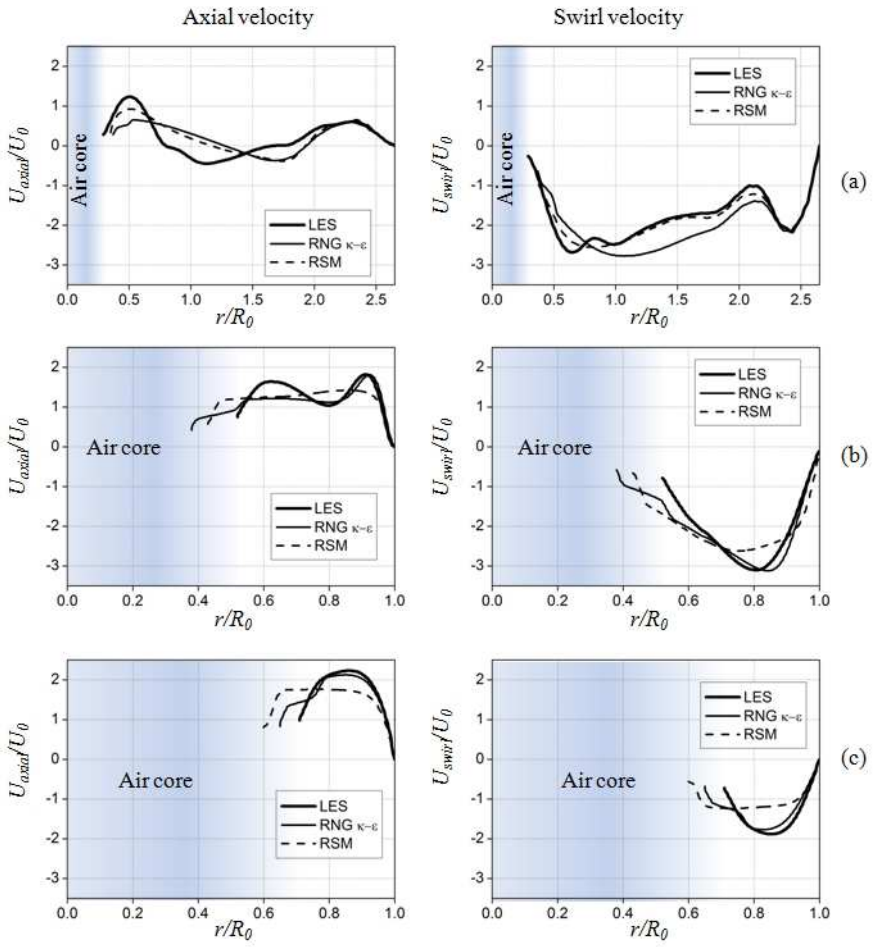

Fig. 7 Radial profiles of three velocity components at three planes along the nozzle axis: (a) *z/Ro* = 4.4, (b) *z/Ro* = 3.2, (c) *z/Ro* = 0; test case # 1 of Table 1.

The swirl velocity profile at z/R_o = 4.4 shows the presence of the Rankine combined vortex structure (as found by Donjat and Estivalezes [5]), with one significant peak close to the wall, which is connected to the inlet configuration investigated here. This phenomenon disappears in the velocity profiles extracted in the other two planes, confirming the strong influence of the inlet flow in the first part of the swirl chamber, with an intense dissipation as the flow moves downward along the injector due to combined effect of frictional losses and change of section.

The comparison of the results obtained with different turbulence models reveals that the LES and the RNG k-ε models predict similar flow fields, with respect to the RSM model, and this observation is also confirmed from the average value of the fuel velocity components at the three sections under investigation, as reported in Table 8. At the discharge hole exit (z/R_o = 0) the difference among the LES and RNG results reaches 20% only for the radial velocity, that has a rather small magnitude, while for the axial and the swirl velocities the difference is always less than 10%.

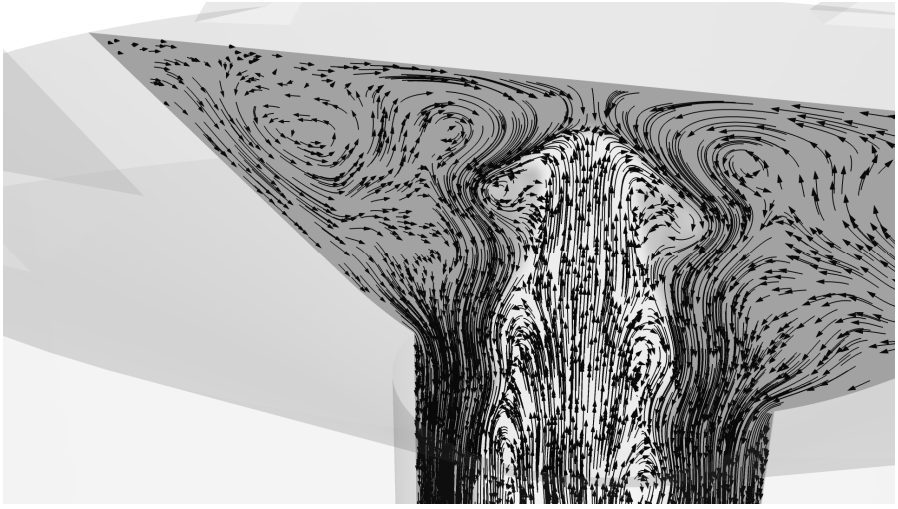

Fig. 8 VOF distribution and flow vector map on a plane along the nozzle axis within the pressure swirl atomizer; test case # 1 of Table 1.

Table 8. Mean velocity components at different planes along the injector axis, predicted by the numerical simulations using three turbulence models

	U_{axial}/U_o			U_{radial}/U_o			U_{swirl}/U_o		
z/R_o	4.4	3.2	0	4.4	3.2	0	4.4	3.2	0
LES	0.203	0.546	1.713	0.141	-0.032	-0.194	1.257	1.967	1.241
RNG k-ε	0.164	0.507	1.745	-0.114	-0.186	0.241	1.333	2.161	1.339
RSM	0.184	0.508	1.541	-0.077	-0.151	0.153	1.203	1.973	1.056

IV. Conclusions

The internal nozzle flow in a pressure swirl atomizer was predicted from fully 3D two-phase flow VOF simulations. Eight operating conditions typical of aeronautical applications, ranging from idle to take off engine operating conditions, have been tested.

The fuel lamella thickness at nozzle exit and the injector discharge coefficient, which are commonly used as standard parameters describing the injector performances, are evaluated from the simulations and compared with the results obtained from correlations available in the literature. The comparison evidenced that the lamella thickness is one of the most difficult parameter to be predicted with good accuracy. The values of lamella thickness and discharge coefficient predicted by the simulations are always within the range of variation of the selected correlations and they are in rather good agreement with some of them.

The effect of turbulence modeling was investigated by comparing the predictions of the lamella thickness, the injector discharge coefficient and the fuel velocity profiles at different planes along the injector axis, *using the LES, RNG k-ε and RSM models*. The results show that the differences among the selected parameters as predicted by the three models are well below the range of variation calculated by the available correlations. Furthermore, the analysis of the flow structures at different sections inside the nozzle shows that the results from the LES and RNG k-ε models *are consistent with each other, while some discrepancies are evidenced by the RSM predictions.*

The analysis presented in this work evidences that the estimation of the principal parameters required by the commonly used atomization models, linking the internal nozzle flow behavior with the spray formation, could be performed by detailed numerical simulations rather than by using correlations derived for different test-cases.

The choice of the turbulence model in the prediction of the internal nozzle flow field and the main parameters characterizing the atomizer behavior does not appear to be so crucial, however this analysis evidences that more

numerical and experimental work will be necessary to better quantify the above mentioned parameters for physically accurate spray numerical modeling.

Acknowledgements

Part of the research leading to these results has received funding from the FIRST Project (FP7/2007-2013) under grant agreement n. 265848.

The authors would like to acknowledge AVIO Group for providing the injector geometry and operating conditions and CINECA for computational resources.

References

1. Walzel, P., "Liquid atomization," *International Chemical Engineering*, Vol. 33, No. 1, 1993, pp. 46-60.

2. Lefebvre, A., *Atomization and sprays*, Vol. 1040, CRC press, 1988.

3. Horvay, M., and Leuckel, W., "LDA-measurements of liquid swirl flow in converging swirl chambers with tangential inlets," *Proceedings of the 2nd International Symposium on Applications of Laser Anemometry to Fluid Mechanics*, 1985, Lisbon, Portugal.

4. Horvay, M., and Leuckel, W., "Experimental and theoretical investigation of swirl nozzles for pressure-jet atomization," *German Chemical Engineering*, Vol. 9, No. 5, 1986, pp. 276-283.

5. Donjat, D., Estivalezes, J.L., and Michau, M., "A description of the pressure swirl atomizer internal flow," *ASME 2002 Joint US-European Fluids Engineering Division Conference*, 2002.

6. Escudier, M.P., Bornstein, J., and Zehnder, N., "Observations and LDA measurements of confined turbulent vortex flow," *Journal of Fluid Mechanics*, Vol. 98, No. 01, 1980, pp. 49-63.

7. Donjat, D., Estivalezes, J.-L., Michau, M., and Lavergne, G., "Phenomenological study of the pressure swirl atomizer internal flow," *Proceedings of 9th ICLASS Conference*, 2003, Sorrento, Italy.

8. Sumer, B., Erkan, N., Uzol, O., and Tuncer, I.H., "Experimental and Numerical Investigation of a Pressure Swirl Atomizer," *Proceedings of 12th ICLASS Conference*, 2012, Heidelberg, Germany.

9. Suyari, M., and Lefebvre, A.H., "Film thickness measurements in a simplex swirl atomizer," *Journal of Propulsion and Power*, Vol. 2, No. 6, 1986, pp. 528-533.

10. Benjamin, M.A., Jeng, S.M., and Jog, M.A., "Comparison of simplex atomizer correlations with detailed CFD and experimental data," *Proceedings of the 10th International Conference on Liquid Atomization and Spray Systems*, 1997, Ottawa, Canada.

11. Jeng, S.M., Jog, M., and Benjamin, M., "Computational and experimental study of liquid sheet emanating from simplex fuel nozzle," *AIAA Journal*, Vol. 36, No. 2, 1998, pp. 201-207.

12. Xue, J., Jog, M.A., Jeng, S.M., Steinthorsson, E., and Benjamin, M.A., "Effect of geometric parameters on simplex atomizer performance," *AIAA Journal*, Vol. 42, No. 12, 2004, pp. 2408-2415.

13. Datta, A., and Som, S.K., "Numerical prediction of air core diameter, coefficient of discharge and spray cone angle of a swirl spray pressure nozzle," *International Journal of Heat and Fluid Flow*, Vol. 21, No. 4, 2000, pp. 412-419.

14. Chinn, J.J., and Yule, A.J., "Computational analysis of swirl atomizer internal flow," *Proceedings of 7th ICLASS Conference*, 1997, New York, USA.

15. Nonnenmacher, S., and Piesche, M., "Design of hollow cone pressure swirl nozzles to atomize Newtonian fluids," *Chemical Engineering Science*, Vol. 55, No. 19, 2000, pp. 4339-4348.

16. Hansen, K.G., Madsen, J., Trinh, C.M., Ibsen, C.H., Solberg, T., and Hjertager, B.H., "A computational and experimental study of the internal flow in a scaled pressure-swirl atomizer," *Proceedings of 18th ILASS-Europe Conference*, 2002, Zaragoza, Spain.

17. Madsen, J., Hjertager, B.H., and Solberg, T., "Numerical simulation of internal flow in a large-scale pressure-swirl atomizer," *Proceedings of 19th ILASS-Europe Conference*, 2004, Nottingham, UK.

18. Yeh, C.-L., "Turbulent flow simulation of liquid jet emanating from pressure-swirl atomizer," *Heat and Mass Transfer*, Vol. 44, No. 3, 2008, pp. 275-280.

19. Hirt, C.W., and Nichols, B.D., "Volume of fluid (VOF) method for the dynamics of free boundaries," *Journal of Computational Physics*, Vol. 39, No. 1, 1981, pp. 201-225.

20. Eswaran, V., *Turbulent flows: fundamentals, experiments and modeling*, CRC Press, 2002.

21. Tonini, S., Galbiati, C., Belotti, A., and Cossali, G.E., "Modelling of spray formation in a pressure swirl atomiser for aircraft engines," *Proceedings of the 26th ILASS-Europe Conference*, 2014, Bremen, Germany.

22. Smagorinsky, J., "General circulation experiments with the primitive equations: I. The basic experiment," *Monthly Weather Review*, Vol. 91, No. 3, 1963, pp. 99-164.

23. Sobel, D.R., and Spadaccini, L.J., "Hydrocarbon Fuel Cooling Technologies for Advanced Propulsion," *ASME Journal of Engineering for Gas Turbines and Power*, Vol. 119, 1997, pp. 344-351.

24. Brackbill, J.U., Kothe, D.B., and Zemach, C., "A continuum method for modeling surface tension," *Journal of Computational Physics*, Vol. 100, 1992, pp. 335-354.

25. Ishak, A., Shaiful, M., Jaafar, M., and Nazri, M., "The effect of swirl number on discharge coefficient for various orifice sizes in a burner system," *Jurnal Mekanikal*, Vol. 17, 2004, pp. 99-108.

26. Rizk, N.K., and Lefebvre, A.H., "Internal flow characteristics of simplex swirl atomizers," *Journal of Propulsion and Power*, Vol. 1, No. 3, 1985, pp. 193-199.

27. Giffen, E., and Muraszew, A., *The Atomization of Liquid Fuels*, Chapmann & Hall, London, 1953.

28. Jedelsky , J., and Jícha, M., "Energy considerations in sprays process of a spill-return pressure-swirl atomizer," *Applied Energy*, Vol. 132, 2014, pp. 485-495.

29. Carlisle, D.R., "Communication on the Performance of a Type of Swirl Atomizer," *Proc. I. Mech. E*, Vol. 169, 1955.

30. Taylor, G.I., "The boundary layer in the converging nozzle of a swirl atomizer," *The Quarterly Journal of Mechanics and Applied Mathematics*, Vol. 3, No. 2, 1950, pp. 129-139.

31. Babu, K.R., Narasimhan, M.V., and Narayanaswamy, K., "Correlations for Prediction of Discharge Rate, Core Angle and Air Core Diameter of Swirl Spray Atomizers," *International Journal of Turbo and Jet Engines*, Vol. 7, No. 3-4, 1982, pp. 235-244.

32. Radcliffe, A., "The performance of a type of swirl atomizer," *Proc. Inst. Mech. Engrs.*, Vol. 169, 1955, pp. 93-106.